Advanced Composites and Hybrid Materials (2021) 4:1185–1204
https://doi.org/10.1007/s42114-021-00353-7

ORIGINAL RESEARCH

Synthesis of GO/HEMA, GO/HEMA/TiO_2, and GO/Fe_3O_4/HEMA as novel nanocomposites and their dye removal ability

Omid Moradi[1] · Mohammad Ali Madanpisheh[2] · Maryam Moghaddas[2]

Received: 2 July 2021 / Revised: 16 September 2021 / Accepted: 17 September 2021 / Published online: 20 October 2021

Abstract
In the present study, the adsorption removal of anionic (MO) and cationic (MB) dyes with GO/HEMA and GO/HEMA/TiO_2 and GO/Fe_3O_4/HEMA nanocomposites as adsorbents was investigated. Characterization of properties was determined by FTIR, XRD, SEM, TEM, EDX, and zeta potential analysis. Parameters affecting the removal of pollutants including dye concentration (0.7 mg/l), contact time (60 min), and temperature (298 °K) were investigated. Pollutants removal mechanisms were studied with pseudo-first-order, pseudo-second-order kinetic models as well as Freundlich Langmuir isotherms. Pollutant removal for all three composites was confirmed by the Freundlich isotherm ($R^2 = 0.99$) and first-order kinetics ($R^2 = 0.98$).

Keywords Synthesis · Characterization · GO nanocomposite · Dye removal ability

1 Introduction

Extensive use of dyes and chemical compounds in various industries around the world has led to serious pollution of water and the environment [1]. Textile dyes are generally classified into two categories: ionic (anionic and cationic) and nonionic (dispersed) [2]. In addition to being toxic and carcinogenic, dyes used in the textile industry cause genetic mutations, which makes it important to remove them from wastewater and other water sources. In addition to the mentioned effects of methylene blue dye, side effects such as eye irritation, nausea, diarrhea, and vomiting have been reported in wastewater containing this dye on humans [3, 4].

Organic dyes are widely used in the textile, printing, plastic, rubber, paper, leather, cosmetics, and pharmaceutical industries [5]. Almost half of the textile dye products are azo compounds whose molecular structure has a chromophore group N = N [6]. Azo dyes are not easily degraded due to their chemical and biological stability, so they must be removed before being discharged into water [7]. Wastewater containing anionic dyes has a net negative charge due to the presence of sulfonate (SO_3^-) groups, while cationic dyes containing protonated sulfur or amine (NH_2) have a net positive charge, so they need to be treated before being discharged to aqueous media [8]. The reason for excellent efficiency, ease of operation, and cost-effectiveness is one of the most effective adsorption processes for liquid or gas phases, which has been considered by many researchers [9].

Dye removal from industrial wastewater by various methods such as various physicochemical [10] methods, surfactant-assisted nanoparticles [11], ion exchange [12], coagulation [13], reverse osmosis [14], and adsorbents such as graphitic carbon nitride (g-C3N4) [15], zeolite [16], silica gel [17], and other studies [18] have been performed. Recently, extensive research has been conducted on the removal of these wastewater, using photocatalytic [18] and wastewater treatment [19] materials, which are a bio-friendly method without any secondary contamination.

GO, which has a high distinct surface area and specific functional groups like the epoxy, carboxyl, and hydroxyl groups at ends of its sheets, demonstrates the high potential for uranium adsorption [20–24].

Various studies have been performed to functionalize GO based on nanomaterials, for various applications with materials such as Au, Ag, ZnO, 2-hydroxyethyl methacrylate (HEMA), and TiO_2 [20, 21]. TiO_2 is used as a nanocomposite adsorbent for wastewater treatment due to its high efficiency, low cost and toxicity, and excellent physical and chemical stability, and the overall TiO_2 efficiency is greatly

✉ Omid Moradi
o.moradi@qodsiau.ac.ir

[1] Department of Chemistry, Shahr-E-Qods Branch, Islamic Azad University, Tehran, Iran

[2] Department of Chemistry, Safadasht Branch, Islamic Azad University, Tehran, Iran

affected by its particle size, crystal structure, porosity, and surface area [22]. Fe_3O_4 has been considered by many researchers due to its high flexibility, ultra-magnetic properties, and low curie temperature, as well as the presence of magnetic nanoparticles in the structure of Fe_3O_4 leading to reduced toxicity and excellent chemical stability [23, 24] and many other applications [25].

In this study, graphene oxide (GO)–based nanocomposites were synthesized using Fe_3O_4, HEMA, and TiO_2. Properties were also characterized by FTIR, XRD, SEM, TEM, EDX, and zeta potential analysis. The nanocomposite materials used in this study were synthesized at room temperature and used as an adsorbent to remove pollutants from aqueous solutions. The effect of important parameters on the removal efficiency of pollutants from aqueous solutions including initial dye concentration, temperature, and contact time was examined. In addition, the pollutant removal mechanisms were studied with Freundlich, Langmuir, and isotherms, as well as the pseudo-first-order and pseudo-second-order kinetic models.

2 Experimental

2.1 Materials

Figure 1 shows the chemical structure of methyl orange (MO) and methylene blue (MB) dyes. Graphene oxide (GO) nanoparticles (99.0%, 3.4–7 nm, 6–7 layers) and Fe_3O_4 nanoparticles (99.5% and 20–30 nm) were purchased from the US Research Nanomaterials Company. TiO_2 nanoparticles were purchased from EVONIK.In. Acetone (COC_2H_6) and ethanol (C_2H_5OH) were purchased from Hamonteb, hydrochloric acid (HCL) from Ghatran shimi, hydrazine monohydrate

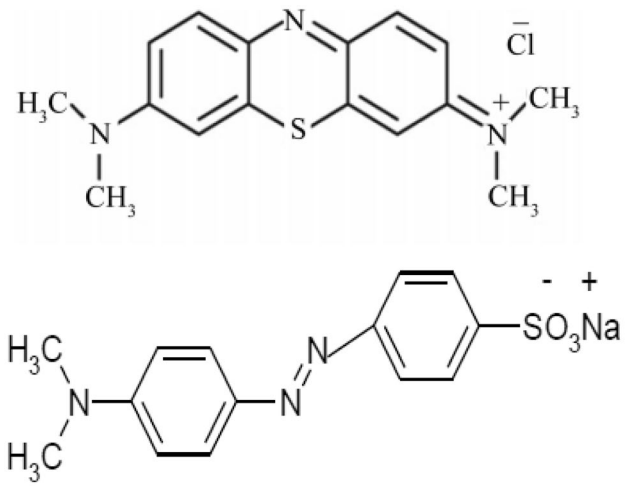

Fig. 1 Chemical structure of methylene blue **a** and methyl orange **b** dyes

(H_6N_2O), sodium disulfate ($Na_2O_5S_2$), and 2-hydroxyethyl methacrylate ($C_6H_{10}O_3$) from Merck, and azobase isobutyronitrile (AIBN) was taken from Sigma-Aldrich.

2.2 Synthesis

2.2.1 Synthesis of nanocomposites GO/HEMA

0.1 g of graphene oxide was added to 100 ml of deionized water and placed in an ultrasonic bath for 1 h. By bringing the temperature of the mixture to 80 °C and after 1 h at the same temperature, 2 g of SDS was added to it, and under the mentioned time and temperature, it was subjected to a magnetic stirrer. Then, 0.5 g of AIBN and 15 g of HEMA were added drop by drop to the above mixture, and 5 drops of pure ethanol were added for 10 min in an ultrasonic bath and then the mixture was stirred for 30 min with a magnetic stirrer then for 6 h. The clock was refluxed at 80 °C. After 6 h, 11 g of H6N2O was added to the mixture and continued for 16 h under reflux at the same temperature. After this time, it was washed by adding 0.1 M HCL solution. The resulting precipitate was washed several times with deionized water to remove SDS and finally dried for 72 h in an oven at 60 °C.

2.2.2 Synthesis of nanocomposites GO/TiO_2

One-step colloidal mixture method was used for the synthesis of GO/TiO_2 nanocomposite. In this method, first 0.3 g of GO in 300 ml of deionized water was added and placed in an ultrasonic bath for 45 min, then 0.3 g of TiO_2 P25 was poured into a container containing GO and placed in an ultrasonic bath for 90 min. The homogenized mixture was then stirred with a magnetic stirrer for 1 h. After several washes at 40 °C, it was dried for 48 h.

2.2.3 Synthesis of nanocomposites GO/TiO_2/HEMA

The GO/TiO_2 suspension was subjected to ultrasonic waves for 45 min. Then, by adding deionized water, the volume of suspension was increased to 500 ml, and 4 g of SDS was added to it. The resulting mixture was stirred for 1 h by a magnetic stirrer at 80 °C. Then, 0.2 g of AIBN was added to the mixture, and also 25 g of HEMA drop by drop was added to the above mixture while stirring; meanwhile, 5 drops of ethanol was added to it. Then, it was refluxed for 6 h at 80 °C. After this period, 15 g of H6N2O was added to the above mixture, and reflux operation was continued at 80 °C for 16 h. By adding 0.1 M HCL solution, the precipitate was washed several times with deionized water to remove SDS and finally dried in an oven at 60 °C for 72 h.

2.2.4 Synthesis of nanocomposites GO/Fe_3O_4

GO/Fe_3O_4 nanocomposite was synthesized by co-precipitation method. First, 0.3 g of GO was added to 300 ml of deionized water and placed in an ultrasonic bath for 45 min. Then, 0.3 g of Fe3O4 was added to it and placed at 50 °C for 5 h by magnetic stirring. Finally, it was washed several times with deionized water.

2.2.5 Synthesis of nanocomposites GO/Fe_3O_4/HEMA

The GO/Fe_3O_4 nanocomposite suspension was subjected to ultrasonic waves for 45 min. Then, by adding deionized water, the volume of suspension was increased to 500 ml, and 4 g of SDS was added to it. The resulting mixture was stirred for 1 h by a magnetic stirrer at 80 °C. After this period, 0.2 g of AIBN was added to the mixture, then 25 g of HEMA was added drop by drop to the mixture while stirring with a magnetic stirrer. Meanwhile, 5 drops of ethanol were added, then refluxed for 6 h at 80 °C. After this period, 15 g of hydrazine monohydrate was added to the above mixture, and the reflux operation was continued at 80 °C for 16 h, then the resulting mixture was washed with 0.1 M HCL solution and the precipitate was removed. The precipitate was washed several times with deionized water to remove SDS, and the precipitate was dried in an oven at 60 °C for 72 h.

2.3 Characterization of nanocomposites

The functional groups present in nanocomposite materials GO, GO/Fe_3O_4, GO/TiO_2, HEMA, GO/HEMA, GO/HEMA/TiO_2, and GO/HEMA/Fe_3O_4 were investigated by FTIR (Perkin Elmer Spectrum 400) in the span of 4000–400 cm^{-1}. X-ray diffraction (XRD) patterns were recorded to detect the crystalline phase with the device D6792-PHILIPS under copper irradiation conditions. SEM (JSM 6400) and TEM were used to determine the morphology and size of the synthesized nanocomposites. Analysis of elements in synthase nanocomposites was performed by energy dispersive X-ray (EDX). Zeta potential (Zetasizer Nano ZEN 3600) was used to measure the surface charge of nanocomposite materials at different pHs.

2.4 Dye adsorption experiment

The adsorption of anionic dye methyl orange (MO) and cationic methylene blue (MB) was performed using synthesized nanocomposite adsorbents. The concentration of dye molecules remaining in solution before and after adsorption was measured using a UV–visible spectrophotometer. The maximum absorbance wavelength for the anionic dye methyl orange 464 nm and the cationic methylene blue 663 nm appeared. All adsorption experiments were performed at ambient temperature in a 100-ml Erlenmeyer with specified concentrations of different adsorbents. In this study, various conditions and factors affecting the adsorption process such as (pH = 7), adsorbent dose of 0.01 g, and contact time (5–60 min) were investigated. The pH of the dye solutions was adjusted by the addition of NaOH and HCL. Removal percentage ($R\%$), adsorption capacity (mg/g) q_t for dyes at time t (min), and the adsorption capacity at equilibrium (mg/g) q_e were calculated from the following equations, respectively [26].

$$R\% = \frac{(C_0 - C_t)}{C_0} * 100 \tag{1}$$

$$q_t = \frac{(C_0 - C_t)V}{m} \tag{2}$$

$$q_e = \frac{(C_0 - C_e)V}{m} \tag{3}$$

where C_0 (mg/L) and C_e (mg/L) are the initial dye concentration and are in equilibrium, respectively, V (L) volume of media and m (g) adsorbent mass are used.

3 Results and discussion

3.1 Characterization of nanocomposite

3.1.1 FTIR

In order to investigate the synthesis of nanocomposite materials and type of functional groups, FTIR spectra obtained in 4000–450 cm^{-1} and provided in Fig. 2a–g. The FTIR spectrum of GO is shown in Fig. 2a. The peak in 3425.37 cm^{-1} is corresponding to the OH functional group, the peaks in 1744 cm^{-1} belong to the functional group C = O, and the peak in 1568.18 cm^{-1} corresponds to C = C GO aromatic surface. The peak in 1208.09 cm^{-1} is related to COC and COH. The peaks in 2921.60 and 2852.04 cm^{-1} are related to CH bending vibrational [27, 28, 29]. The FTIR spectrum of GO/Fe3O4 nanocomposite is shown in Fig. 2b. The 583 cm^{-1} band is related to the vibration of the Fe-O bond in Fe3O4 attributed to GO/Fe3O4 nanocomposite. In this spectrum, the band 1221 cm^{-1} corresponds to the C-N bond. The band of 1571 cm^{-1} indicates the tensile and bending vibrational of the N-H band on the surface of GO. The broad band observed at 3386 cm^{-1} may be related to the O-H tensile vibration of H2O adsorbed on the GO/Fe3O4 surface [30]. Figure 2c shows the FTIR spectrum of GO/TiO2 nanocomposite. The bands 3431 and 1574 cm^{-1} represent the tensile

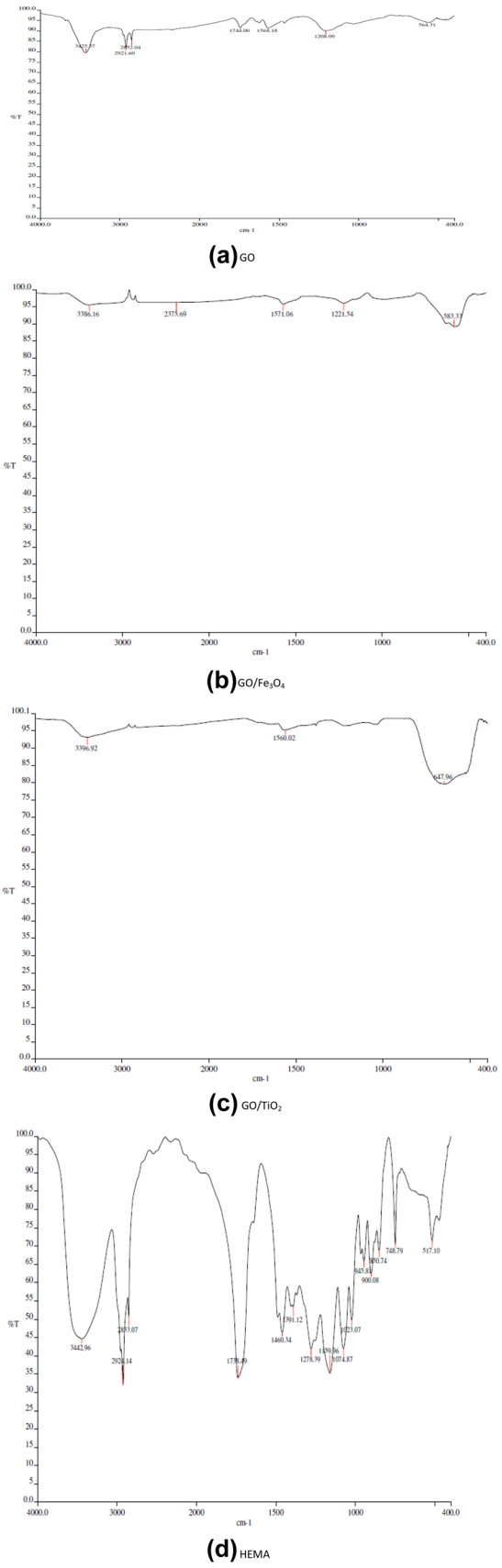

Fig. 2 FTIR spectra of **a** GO; **b** GO/Fe_3O_4; **c** GO/TiO_2; **d** HEMA; **e** ▶ GO/HEMA; **f** GO/HEMA/TiO_2; and **g** GO/HEMA/Fe_3O_4

and bending vibrational of the O-H band, respectively, while the strong uptake at 580–617 cm^{-1} is related to the tensile vibrations of Ti-O in TiO2 [31]. The FTIR spectrum of HEMA is shown in Fig. 2d. The strong peak in 3442.96 cm^{-1} belongs to the OH functional group in the OH and COOH groups. The peaks in 2924.14, 2853.07, and 1391.12 cm^{-1} are related to the bending vibrations of C-H bond of methylene and methyl groups. The peaks in 1278, 1159, 1074, and 1023 cm^{-1} belong to the C-O bond belonging to the ester and OH groups. Figure 2e shows the FTIR spectra of the GO/HEMA nanocomposite. The strong peak in 3441 cm^{-1} belongs to the OH functional group; the C=O group, which has been functionalized and produced the carboxylic group (COOH), has a peak of 1735 cm^{-1}, and an COC bond in 1156 cm^{-1} and an alcoholic C-OH in 1459 cm^{-1} and 1405 cm are related to the C=C aromatic bond of GO surface. Clear peaks of HEMA are observed in areas 2923, 2852, and 1365 cm^{-1}, which are related to the flexural vibrations of the C-H bond of the methylene and methyl groups. The peaks of 900, 945, 850, and 748 cm^{-1} are related to the flexural vibrations outside the aromatic plate, or the bending vibration outside the CH surface is alkaline. The GO/HEMA/TiO2 nanocomposite has a common feature with the GO/HEMIA nanocomposite, so the peaks shown in both cases have considerable similarities. As shown in Fig. 2f, the FTIR spectra of the GO/HEMA/TiO2 nanocomposite, the strong peak in 3441 cm^{-1} is related to alcoholic OH, and the peaks of 2954 and 1391 cm^{-1} are related to the bending vibrations of the C-H bond in the methyl and methylene groups. The peaks of 1457 and 1488 cm^{-1} belong to the aromatic groups of GO surface. Peaks of 1276 and 1156 cm^{-1} are related to C-O alcohol and C-O ester of GO plates, respectively. The peaks of 945, 900, 850, and 748 cm^{-1} are related to extra-aromatic vibrations, and the peak of 519 cm^{-1} belongs to C-Ti. The GO/HEMA/Fe3O4 nanocomposite FTIR spectrum is very similar to the GO/HEMA/TiO2 nanocomposite FTIR spectrum because most of the bonds in both nanocomposites are almost identical [23, 32]. As shown in Fig. 2g, the FTIR spectra of the GO/HEMA/Fe3O4 nanocomposite, the peak in 3434 cm^{-1} corresponds to O-H alcohol; the peaks in 2925, 2853, and 1391cm^{-1} belong to the methyl and methylene groups. The peaks of 1486 and 1455 cm^{-1} are related to the C=C bonds of GO plates. The peaks of 1278 and 1160 cm^{-1} are related to C-O alcohol and ester of GO plates, respectively. The peaks of 945, 899, 851, and 748 cm^{-1} are related to the bending vibrations outside the aromatic plate of graphene oxide filters, and the peak of 521 cm^{-1} belongs to the C-Fe bond [33-39].

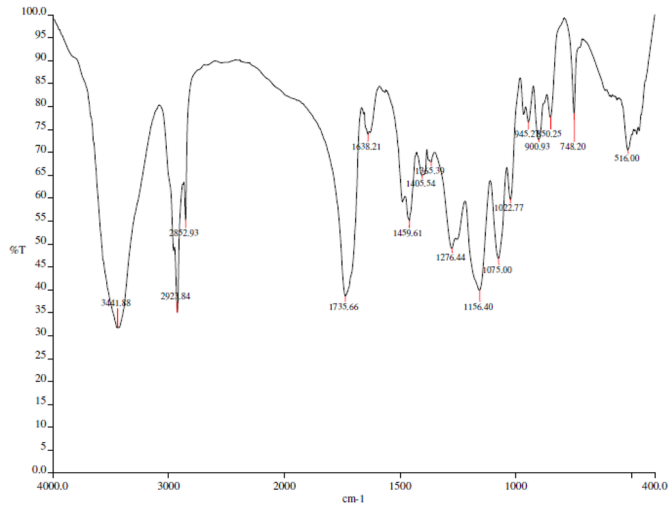

(e) GO/HEMA

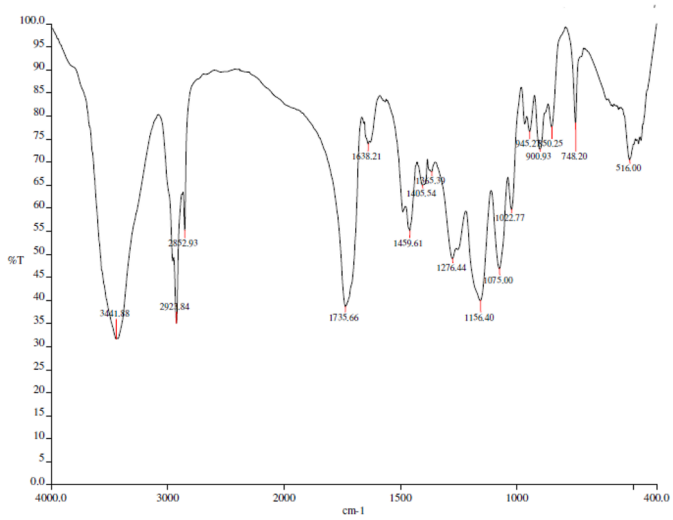

(f) GO/HEMA/TiO_2

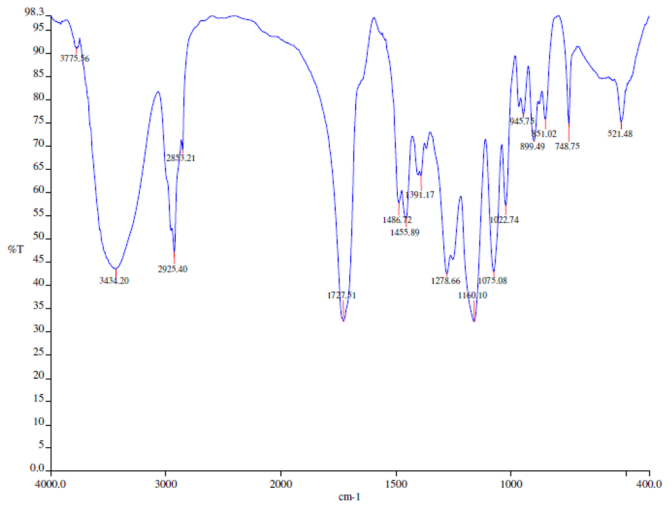

(g) GO/HEMA/Fe_3O_4

Fig. 2 (continued)

3.1.2 XRD

The XRD pattern of the synthesized nanocomposite materials is presented in Fig. 3a–e. The XRD, GO spectrum, is shown in Fig. 3 at which corresponds to the previously reported work [28]. According to Fig. 3b, it is obvious that the XRD spectrum of HEMA consists of a very wide peak, which indicates the amorphous morphology of HEMA, and is related to the polymeric structure of the material [28, 30]. The XRD GO/HEMA sample can be seen in Fig. 3c. Due to the presence of the HEMA polymer substrate and the formation of a wide peak, and as a result of its amorphous peak, other elements and phases are covered by it, which can be due to high energy effect XRD on HEMA polymer [20]. Like the XRD pattern of HEMA and GO/HEMA, which have a wide peak due to the structure of the polymer base, so that the phase of other materials is covered. In the XRD spectra of GO/HEMA/Fe3O4 in Fig. 3d and GO/HEMA/TiO2 nanocomposites Fig. 3e, they are also wide due to the peak polymer substrate, so the XRD spectrum cannot be used to determine the structure of these nanocomposites, which is in accordance with previously reported work [26, 40].

3.1.3 SEM and TEM

Figure 4a–c shows scanning electron microscope (SEM) images of synthesized nanocomposite materials. Figure 4a shows the GO/HEMA scanning electron microscope image. As shown in Fig. 4a, the HEMA polymer matrix is uniformly placed on the graphene oxide surface. According to Fig. 4b, dimensions below 100 nm indicate

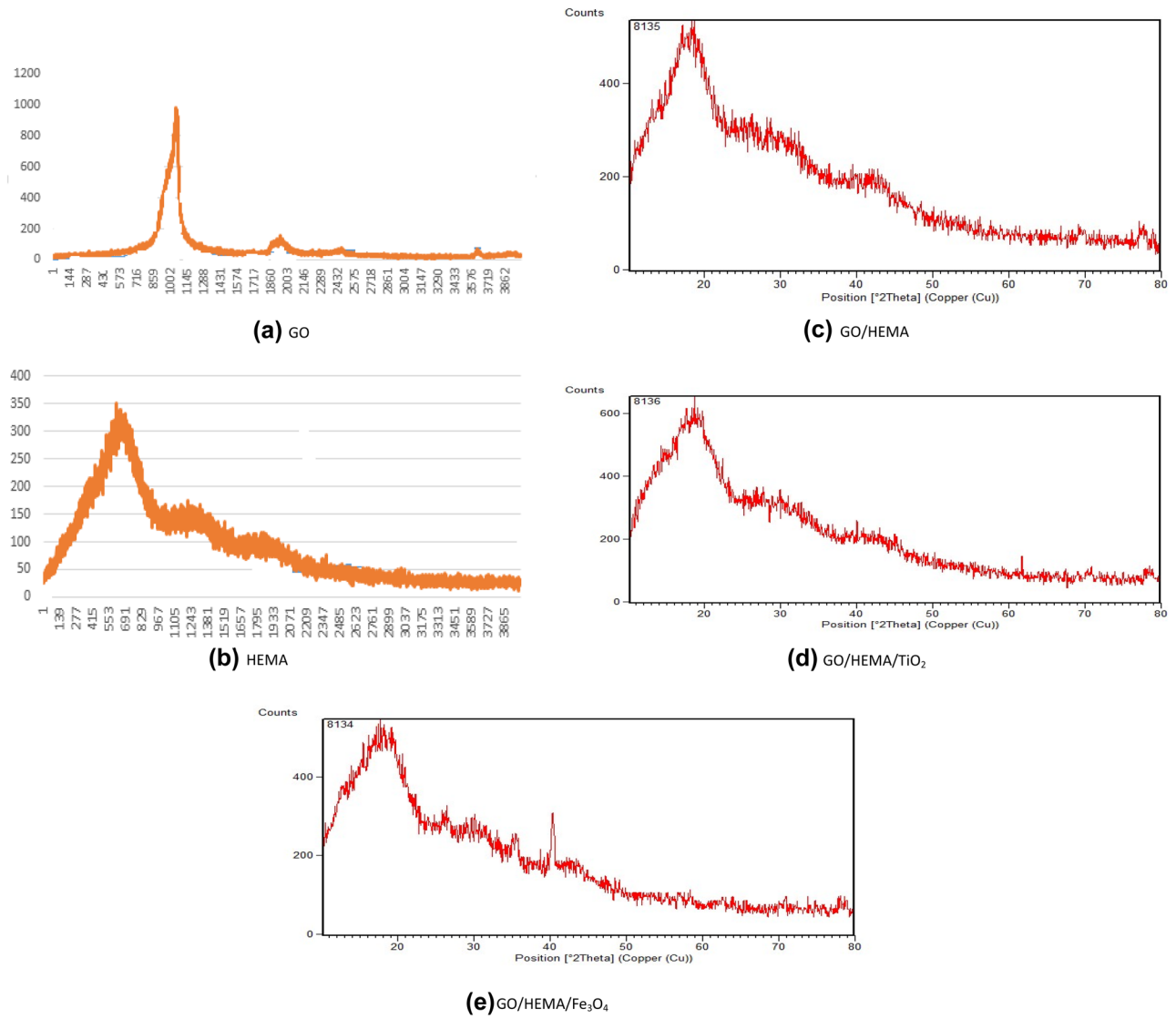

Fig. 3 XRD analysis of **a** GO; **b** HEMA; **c** GO/HEMA; **d** GO/HEMA/TiO_2; and **e** GO/HEMA/Fe_3O_4

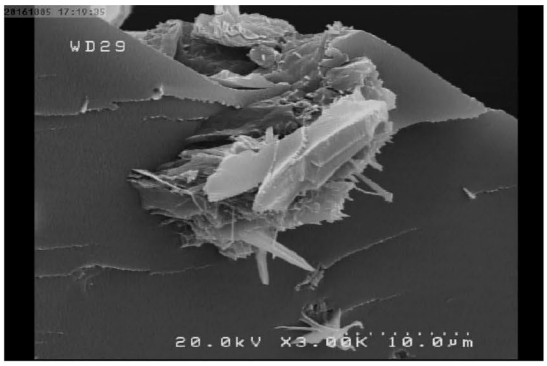

(a) SEM GO/HEMA

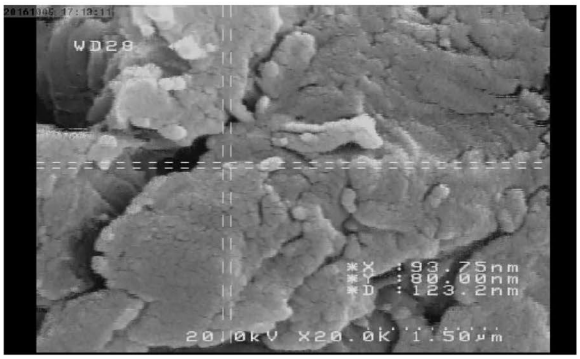

(b) SEM GO/HEMA/TiO_2

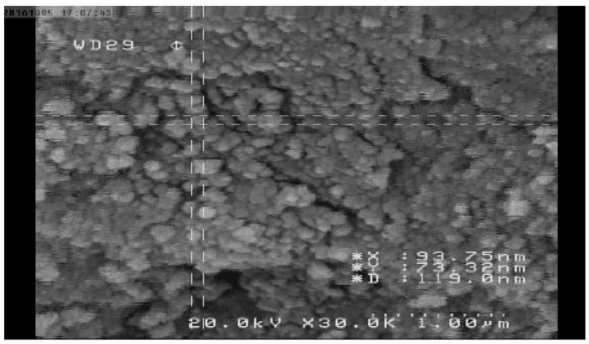

(c) SEM GO/HEMA/Fe_3O_4

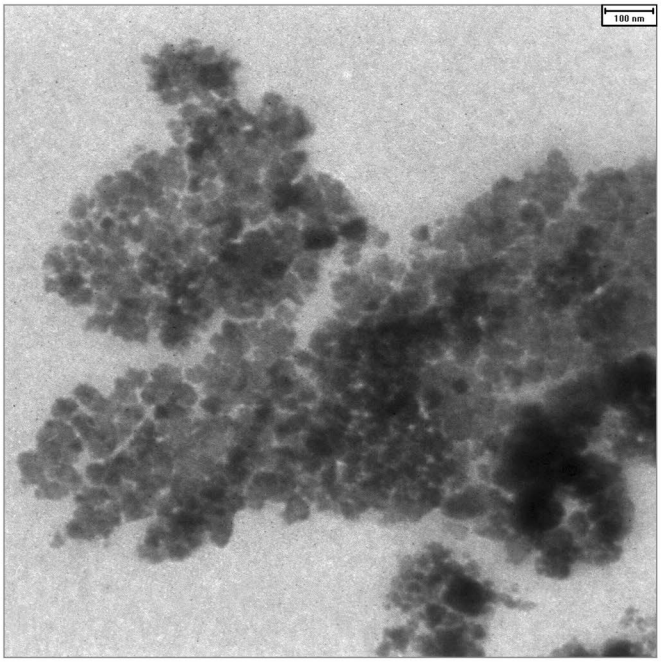

(d) TEM GO/HEMA/Fe_3O_4

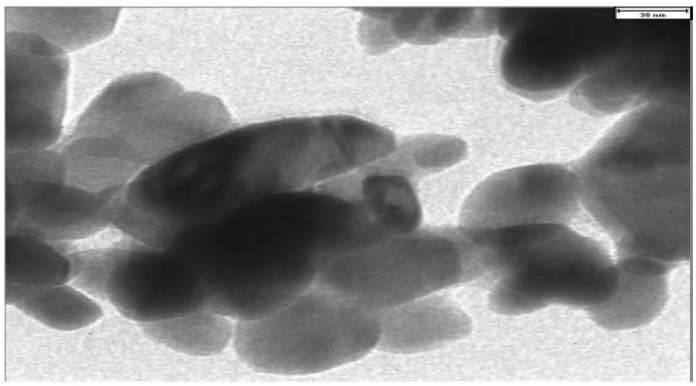

(e) TEM GO/HEMIA/TiO_2.

Fig. 4 SEM images: **a** GO/HEMA, **b** GO/HEMA/TiO_2, and **c** GO/HEMA/Fe_3O_4; TEM images **d** GO/HEMA/Fe_3O_4 and **e** GO/HEMIA/TiO_2

the formation of GO/HEMA/TiO_2 nanocomposite. Figure 4b shows that TiO_2 nanoparticles are formed on GO. According to Fig. 4c, dimensions below 100 nm indicate the formation of GO/HEMA/Fe_3O_4 nanocomposite, which indicates the formation of Fe_3O_4 nanoparticles on GO. In SEM images, all three nanocomposites have gaps on the polymer surface, which is due to the polymeric nature of the nanocomposite substrate, which occurred with increasing device voltage.

The structure size of the synthesized nanocomposites was examined by transmission electron microscopy (TEM). The TEM image of GO/HEMA/Fe3O4 nanocomposite in Fig. 4d shows that the presence of Fe3O4 nanoparticles on GO sheets in the nanocomposite is proved, which indicates a strong relationship between GO sheets and Fe3O4 nanoparticles. According to Fig. 4e, the presence of TiO2 nanoparticles on GO sheets in GO/HEMIA/TiO2 nanocomposite has been proven and indicates the formation of GO/HEMIA/TiO2 nanocomposite, which indicates a strong correlation between GO sheets and TiO2 nanoparticles.

3.1.4 EDX

EDX analysis was used to determine the elements existing in GO/HEMA/TiO_2 and GO/HEMA/Fe_3O_4 nanocomposites.

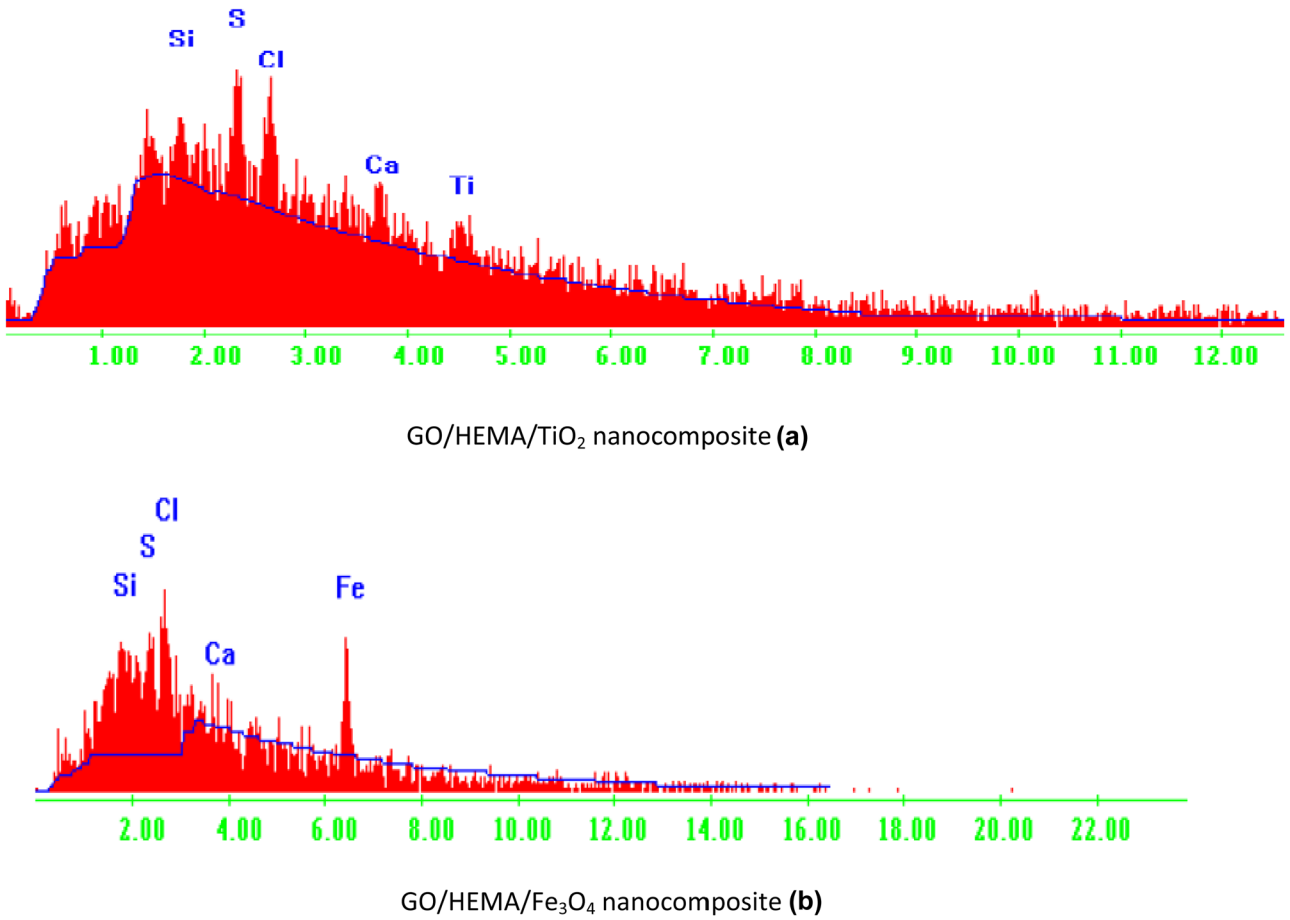

Fig. 5 EDX analysis of GO/HEMA/TiO_2 nanocomposite **a** and GO/HEMA/Fe_3O_4 nanocomposite **b**

Figure 5a EDX analysis of GO/HEMA/TiO_2 nanocomposite shows that the presence of Ti metal element in the structure of this material is obvious. Figure 5b shows the EDX analysis of GO/HEMA/Fe_3O_4 nanocomposite, where the presence of the metal element Fe in the structure of this nanocomposite is distinct [23].

3.1.5 Zeta potential

Zeta potential test was used to measure the surface charge of GO/HEMA, GO/HEMA/Fe_3O_4, and GO/HEMA/TiO_2 nanocomposites at pHs of 5.5, 7, 9, and 10, as shown in Fig. 6a–c. It was found that the zeta potential for GO/HEMA nanocomposite at pHs of 5.5, 7, 9, and 10 with increasing pH generally increased the zeta potential of − 33.5 mv at pH = 3 to − 16.8 mv at PH = 10, which indicates a decrease in negative charge with increasing pH in this nanocomposite. Also, the zeta potential for GO/HEMA/Fe_3O_4 nanocomposite was measured at pHs of 5.5, 7, 9, and 10, and it was found that increasing the pH generally reduced the zeta potential to − 9.5 mv at pH = 3; it changed to − 22.7mv at pH = 10, which indicates an increase in negative charge with increasing pH in this nanocomposite. By measuring the zeta potential for GO/HEMA/TiO_2 nanocomposite at pHs of 5.5, 7, 9, and 10, it was found that with increasing pH, the total zeta potential decreased to − 16.4 mv at pH = 5.5 to − 22.4 mv changed in pH = 10, which indicates an increase in negative charge with increasing pH in this nanocomposite [41–44].

3.2 Pollutant removal

3.2.1 Initial DR23 concentration

In order to investigate the adsorption process, the effect of initial concentration of cationic (MB) and anionic (MO) dyes on GO/HEMA and GO/HEMA/Fe_3O_4 and GO/HEMA/TiO_2 nanocomposites with constant adsorbent dose (0.001 g) and with different concentrations (0.1, 0.3, 0.5, and 0.7 mg/l) was evaluated at pH = 7.0 and at ambient temperature. The results are shown in Fig. 7a–c. With increasing the initial concentration of dye (0.1 to 0.7 mg/l), the rate of dye removal efficiency did not change significantly. During the studies, the nanocomposite synthesized in this study showed a high ability to absorb

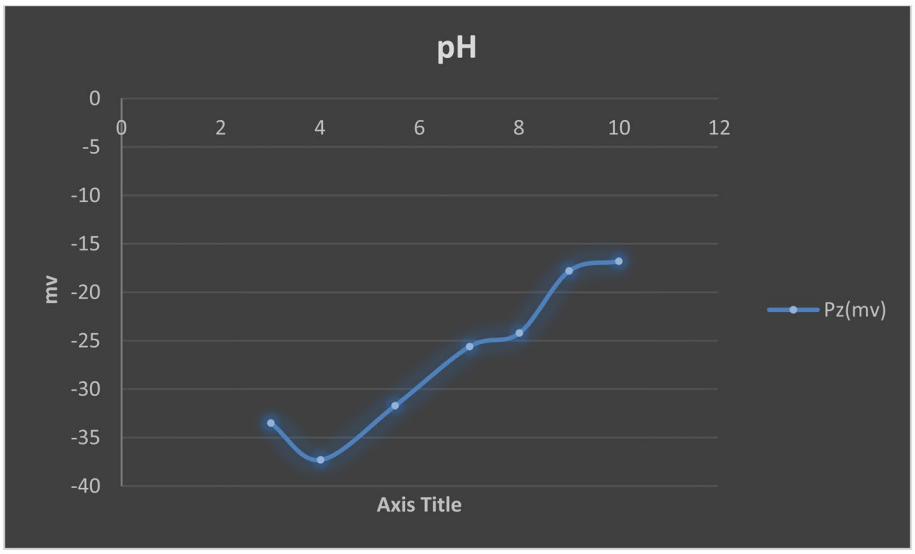

(a) GO/HEMA

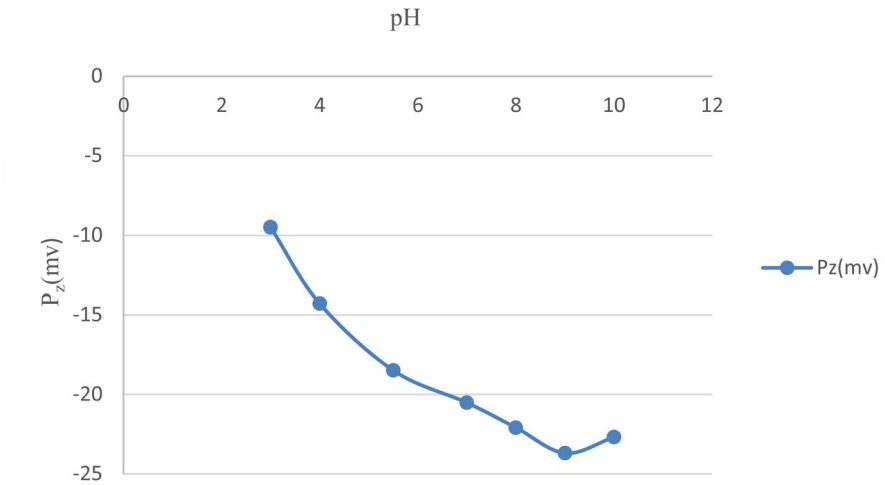

(b) GO/HEMA/Fe_3O_4

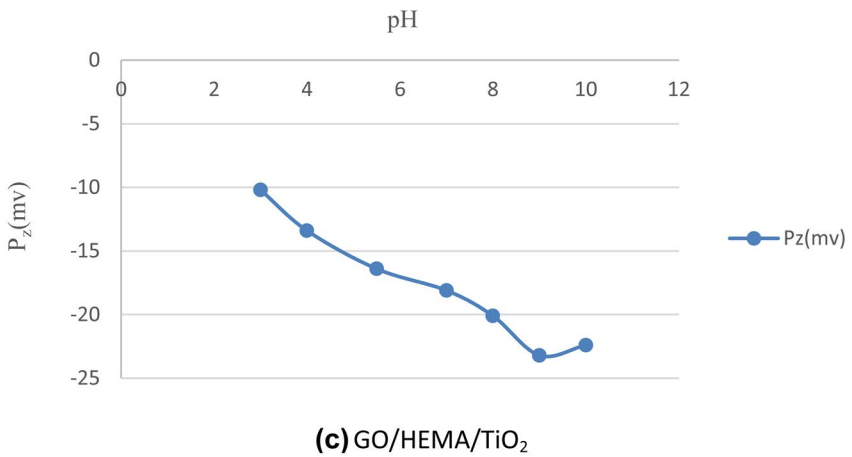

(c) GO/HEMA/TiO_2

Fig. 6 The zeta potential of **a** GO/HEMA; **b** GO/HEMA/Fe_3O_4; and **c** GO/HEMA/TiO_2 under various pH (5.5, 7, 9, and 10)

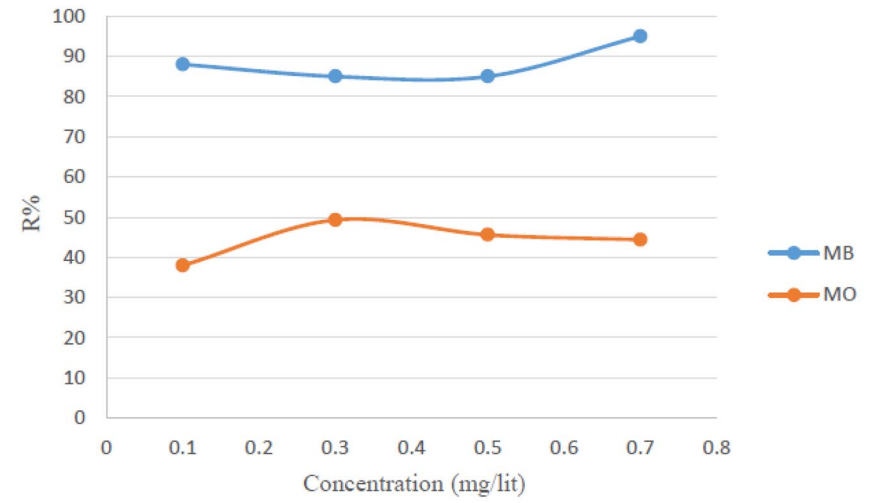

(a) GO/HEMA

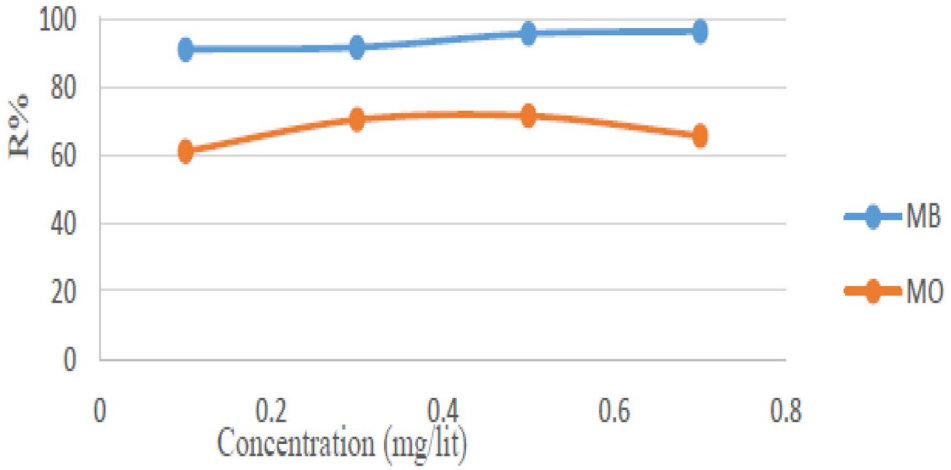

(b) GO/HEMA/Fe_3O_4

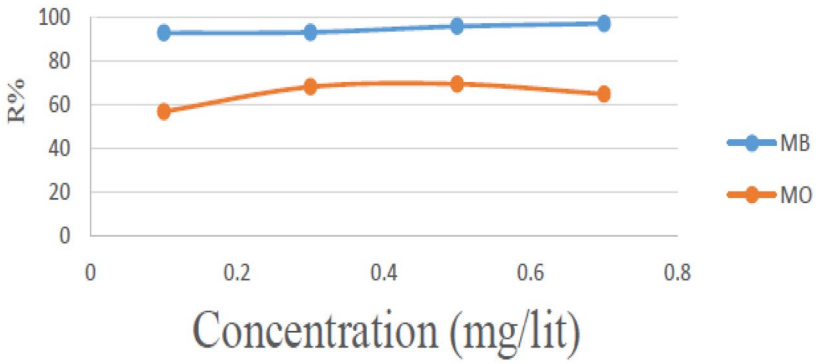

(c) GO/HEMA/TiO_2

Fig. 7 Effect of initial pollutants concentration (0.1, 0.3, 0.5, and 0.7). **a** GO/HEMA; **b** GO/HEMA/Fe_3O_4; and **c** GO/HEMA/TiO_2 on dye removal

the dye in different concentrations. According to Fig. 7a, in the case of GO/HEMA nanocomposites, the maximum adsorption for MB occurred at a concentration of 0.7 mg/l, which is 95%. As the concentration increases, more adsorption sites are used and filled [45, 46], but the maximum adsorption for MO occurs at a concentration of 0.3 mg/l, which was equal to 49.3%.

In the case of GO/HEMA nanocomposites, the max adsorption for MB occurred at a concentration of 0.7 mg/l, which is equal to 95%. But the max adsorption for MO at a concentration of 0.3 mg/l was 49.3%. In the case of GO/HEMA/Fe_3O_4 nanocomposites, the max adsorption occurred at a concentration of 0.7 mg/l which was 96.29%. Also, the max adsorption for MO was obtained at a concentration of 0.5 mg/l and 71.4%, which is shown in Fig. 7b. If the amount of adsorbent does not change significantly with increasing the driving force of the concentration gradient, the amount of contaminant adsorbed on nanocomposites increases with increasing initial dye concentration [47]. For GO/HEMA/TiO_2 nanocomposites as shown in Fig. 7c, the max adsorption at 0.7 mg/l was 97.29% and the max adsorption for MO at initial concentration were 0.3 mg/l and 92.3%. It can be said that in high concentrations, more adsorption sites are used [45, 46].

3.2.2 Adsorption contact time

Factors affecting the adsorption of MB and MO dyes by GO/HEMA, GO/HEMA/Fe_3O_4, and GO/HEMA/TiO_2 nanocomposites at different times of 5–60 min with initial concentration 0.7 ppm and adsorbent dose 0.001 g were investigated. According to the results obtained in Fig. 8a, the maximum dye removal percentage for MB with GO/HEMA nanosorbent at 55 min is 85%. The maximum adsorption for MO dye in the same conditions is 45.6%, which indicates a sharp decrease in adsorption for MO compared to MB. In the case of GO/HEMA/Fe_3O_4 nanosorbent, the maximum adsorption occurred in 35 min, and the maximum adsorption was 95.6%. Also, for MO in the same conditions, the maximum absorption in 55 min is equal to 71.4%, which is presented in Fig. 8b. For GO/HEMA/TiO_2 nanocomposite adsorbent, the maximum adsorption was 96% in 35 min, and for MO under the same conditions, was 55 min and the max adsorption was 69.6%, which is reported in Fig. 8c. Differences in removal percentage and adsorption time can be attributed to the effects of surface charge and type of interactions between nanosorbents and contaminants. The presence of metal oxide nanoparticles increases the electrostatic interaction between nanosorbents and pollutants. According to the results, GO/HEMA/TiO_2 nanocomposite has a max adsorption rate than GO/HEMA/Fe_3O_4 nanocomposite, which seems to be due to the decomposition of MB by GO/HEMA/TiO_2 nanocomposite. As we know, MB molecule is a flat molecule, but MO molecule is a bulky and non-planar molecule, which reduces the electrostatic gravitational forces between MO molecule and nanosorbents. On the other hand, MO is an anionic dye that is the same as the surface charge of nanosorbents in adsorption conditions; therefore, it increases the electrostatic repulsion force, and thus, the amount of adsorption decreases [19, 48, 49].

3.2.3 The effect of temperature on pollutants

The effect of temperature on the synthesized nanocomposites with initial concentration of 0.7 mg/l and pH = 7 and adsorbent dose of 0.001 g at 5 different temperatures was investigated, which is presented in Fig. 9a–c. According to the data, with increasing temperature, the rate and amount of MB and MO dye adsorption by nanocomposites has increased that increasing the percentage of adsorption with increasing temperature indicates that the adsorption process is endothermic. This may be due to the increased mobility of the dye from the solution to the adsorbent surface. Also, with increasing temperature, dye molecules can have enough energy to interaction with active sites [28, 50]. However, as shown by the adsorption percentage diagrams relative to temperature, the adsorption reaction of MB by GO/HEMA nanocomposite is more endothermic.

3.2.4 Adsorption isotherms

The adsorption isotherm at constant temperature expresses the equilibrium value of the adsorbed substance on a solid surface physically or chemically. To analyze the data obtained from the adsorption experiment, Langmuir and Freundlich isotherm models were used, which can investigate the relationship between adsorption capacity and adsorbent concentration in equilibrium. An adsorption equilibrium is established when the amount of dye adsorbed on the adsorbent surface is equal to the amount of dye desorption from the adsorbent surface. The mentioned isothermal models for GO/HEMA (Fig. 10a–d), GO/HEMA/Fe_3O_4 (Fig. 11a–d), and GO/HEMA/TiO_2 (Fig. 12a–d) nanocomposites for MB and MO dyes are shown. In Langmuir model, it is assumed that the adsorption on the sites is homogeneous and is monolayer. The Freundlich model assumes that adsorption is reversible on heterogeneous sites, and this model is suitable for multi-layer adsorption. This model also predicts that as the initial concentration of dye in the solution increases, the initial concentration of dye increases. The degree of compatibility of each isotherm with the process is measured by a correlation coefficient of R^2. In this way, the higher coefficient R^2 of the isotherms is selected as the isotherm compatible with the adsorption process [49, 51, 52].

The Langmuir and Freundlich equations are expressed according to Eqs. (4) and (5) as follows:

$$C_e/q_e = 1/K_l \bullet q_l + C_e/q_l \tag{4}$$

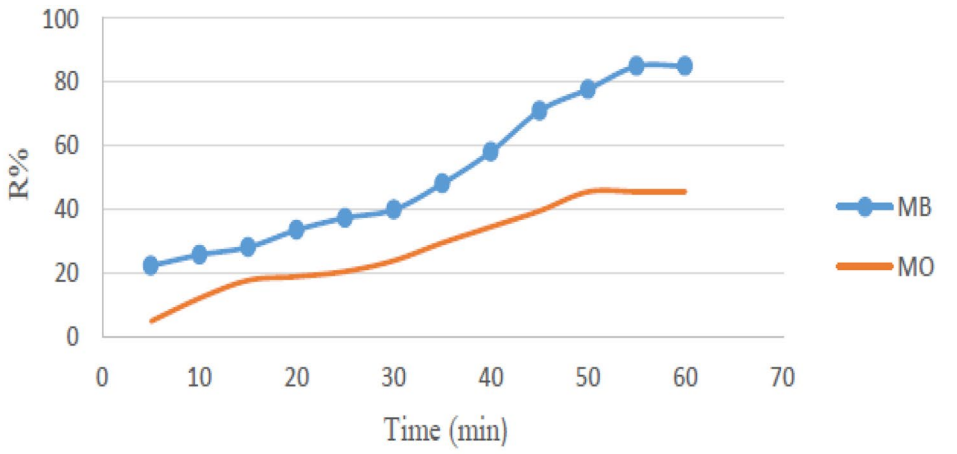

(a) GO/HEMA

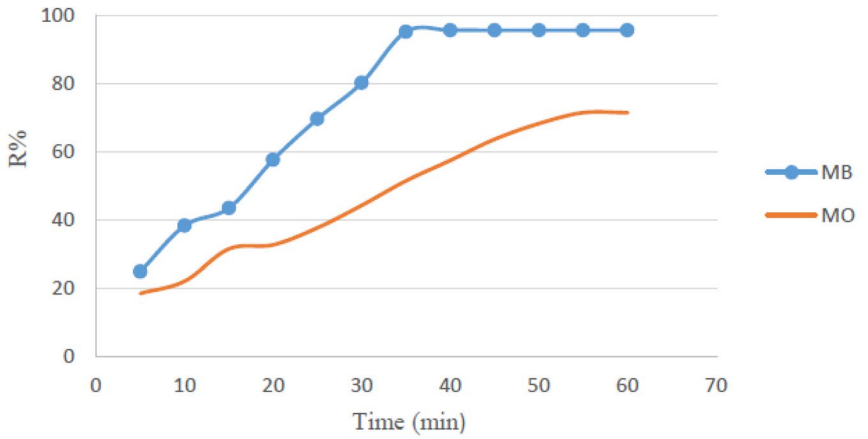

(b) GO/HEMA/Fe_3O_4

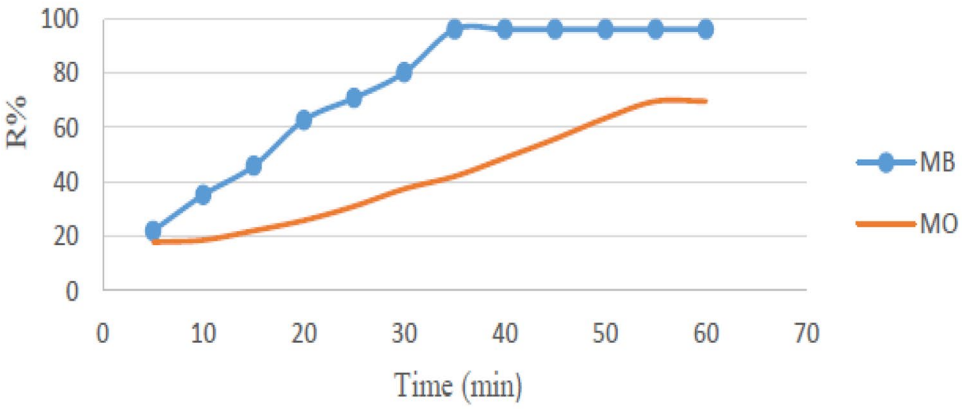

(c) GO/HEMA/TiO_2

Fig. 8 Impact of contact time for MB and MO removal **a** GO/HEMA; **b** GO/HEMA/Fe_3O_4, and **c** GO/HEMA/TiO_2

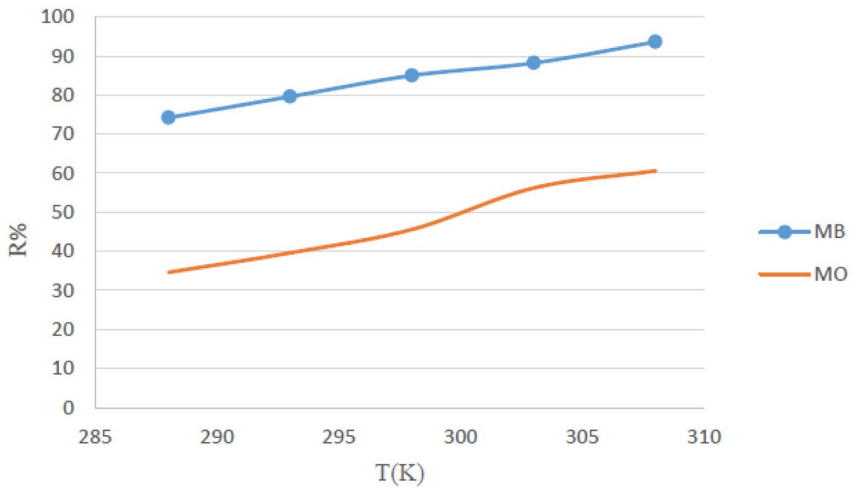

(a) GO/HEMA

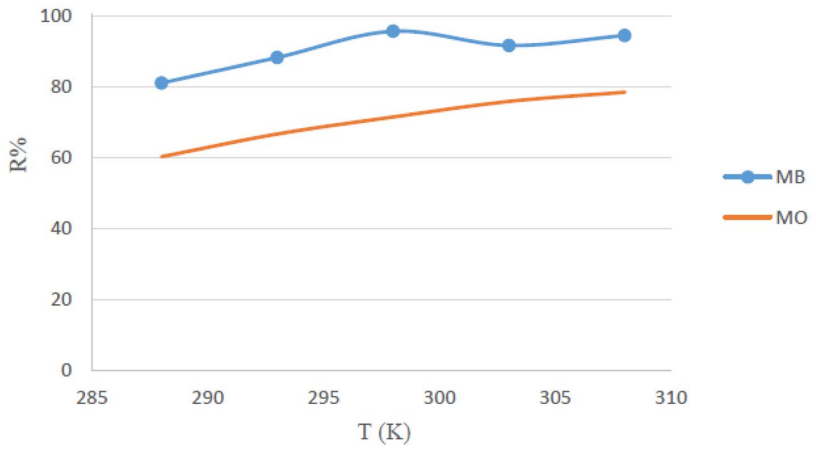

(b) GO/HEMA/Fe_3O_4

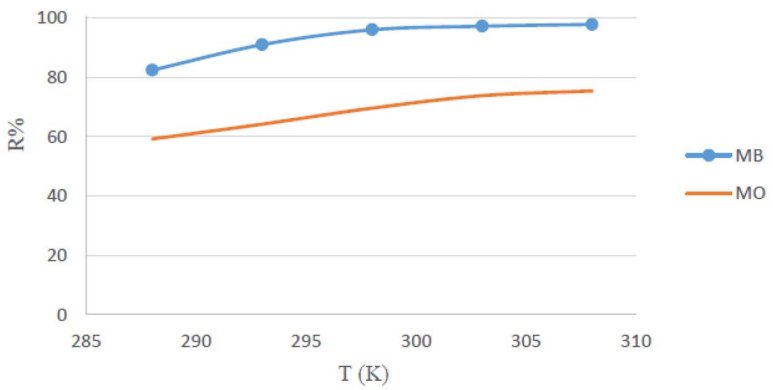

(c) GO/HEMA/TiO_2.

Fig. 9 The effect of temperature on the synthesized nanocomposites **a** GO/HEMA; **b** GO/HEMA/Fe_3O_4; and **c** GO/HEMA/TiO_2

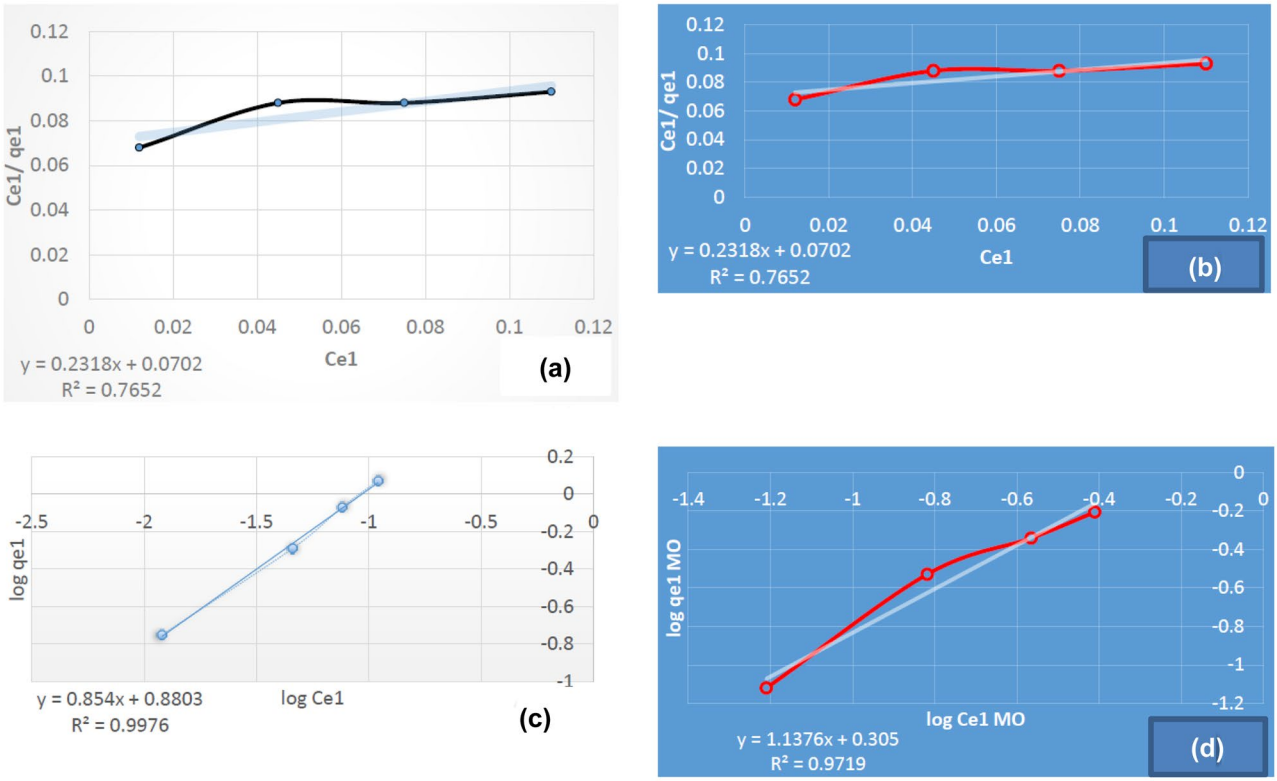

Fig. 10 The Langmuir isotherm nanocomposites GO/HEMA for adsorption: **a** MB and **b** MO; the Freundlich isotherm nanocomposites GO/HEMA for adsorption: **c** MB and **d** MO

In the above relation, q_L in mg/g and constant Langmuir K_L (l/mg) are the adsorption capacity and the adsorption energy, respectively. Also C_e is the equilibrium concentrations of the solution (mg/l); q_e is the adsorption capacity in equilibrium (mg/g).

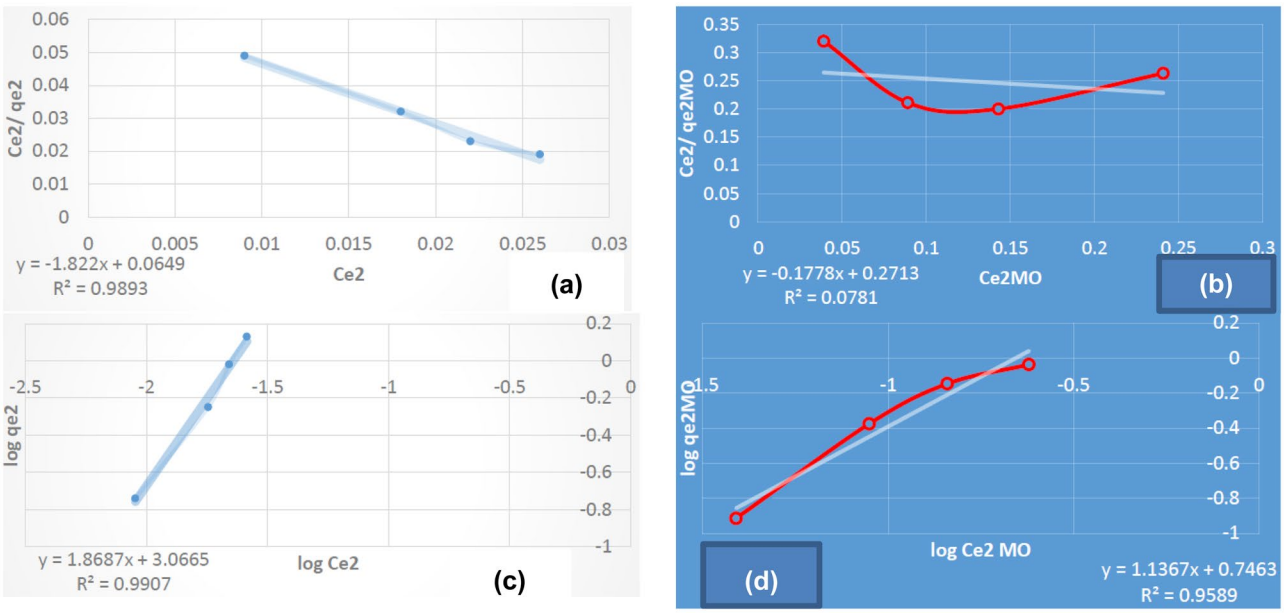

Fig. 11 The Langmuir isotherm nanocomposites GO/HEMA/Fe3O4 for adsorption: **a** MB and **b** MO; the Freundlich isotherm nanocomposites GO/HEMA/Fe3O4 for adsorption: **c** MB and **d** MO

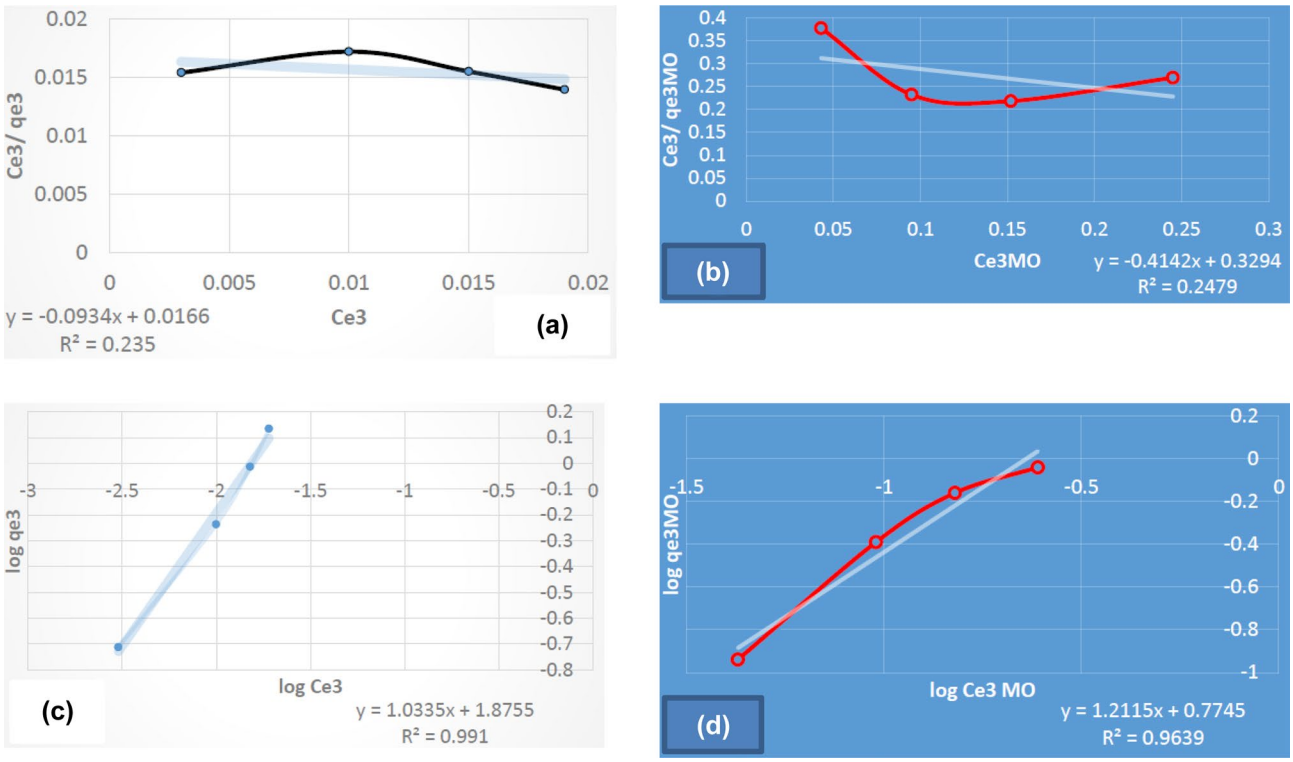

Fig. 12 The Langmuir isotherm nanocomposites GO/HEMA/TiO_2 for adsorption: **a** MB and **b** MO; the Freundlich isotherm nanocomposites GO/HEMA/TiO_2 for adsorption: **c** MB and **d** MO

$$loqqe = loqKf + \frac{1}{n} loqCe \tag{5}$$

In this equation, K_F (L/g) and $1/n$ (mg/L) are coefficients related to adsorption capacity and adsorption intensity, respectively. Values of $1/n$ indicate the type of isotherm if irreversible ($1/n = 0$), desirable ($0 > 1/n < 1$), and undesirable ($1/n > 1$). Also, if $n = 1$, the adsorption decreases linearly; in fact, it becomes independent of concentration (Table 1).

3.2.5 Adsorption kinetics

Adsorption kinetics depends on the physical and chemical properties of the adsorbent that affect the adsorption mechanism. In this research, two pseudo-first-order and pseudo-second-order kinetic models have been selected to investigate the adsorption process. The pseudo-first-order kinetics is assumed that adsorption occurs due to

Table 1 Isotherm parameters for dyes adsorption on nanocomposites materials

Isotherm	Parameter	Adsorbents		
		GO/HEMA	GO/HEMA/Fe3O4	GO/HEMA/TiO_2
MB	q_L	14.314	122.20	109.71
Langmuir	K_L	3.302	28.53	5.625
$C_e/q_e = 1/K_L\, q_L + C_e/q_L$	R^2	0.7652	0.9893	0.235
Freundlich	K_F	7.59	1165.47	75.076
Log q_e = log K_f + 1/n log C_e	n	1.171	0.535	0.967
	R^2	0.9972	0.9907	0.991
MO				
Langmuir	q_L	14.314	115.624	112.414
	K_L	3.302	0.655	1.258
$C_e/q_e = 1/K_L\, q_L + C_e/q_L$	R^2	0.7652	0.9589	0.2479
Freundlich	K_F	2.08	5.576	5.95
	n	0.879	0.88	0.825
Log q_e = log K_f + 1/n log C_e	R^2	0.9719	0.9589	0.9632

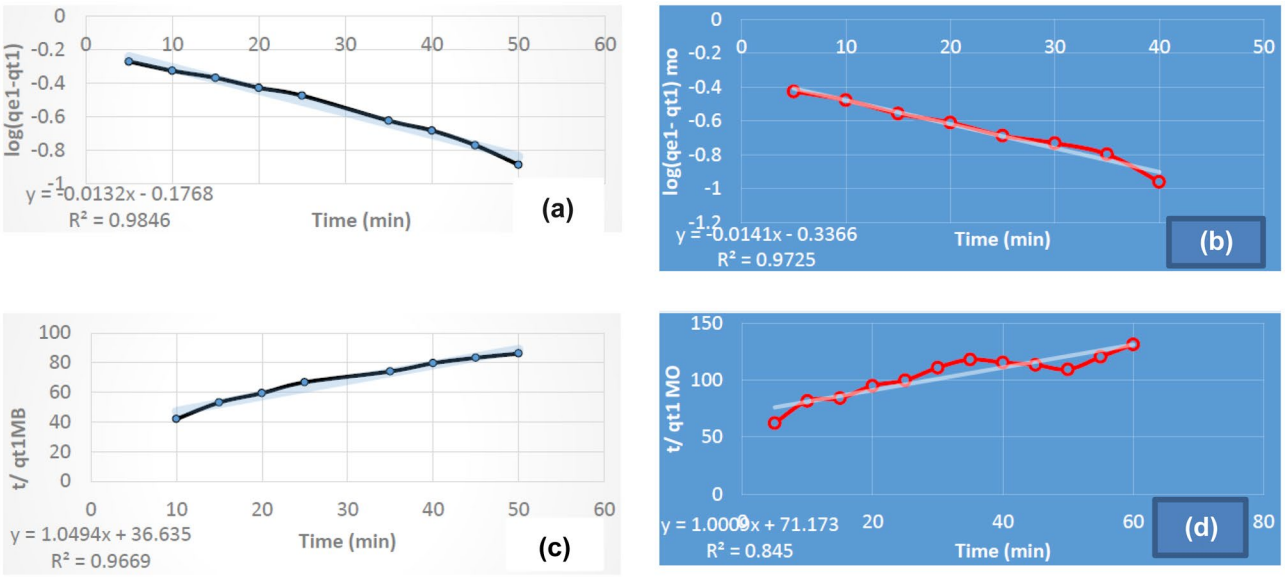

Fig. 13 The pseudo-first-order kinetics nanocomposites GO/HEMA for adsorption: **a** MB and **b** MO; the pseudo-second-order kinetics nanocomposites GO/HEMA for adsorption: **c** MB and **d** MO

the concentration difference between the adsorbent surface and the solution. The mentioned kinetic models for GO/HEMA (Fig. 13a–d), GO/HEMA/Fe_3O_4 (Fig. 14a–d), and GO/HEMA/TiO_2 (Fig. 15a–d) nanocomposites for MB and MO dyes are shown. Kinetic parameters such as absorption capacity in equilibrium (qe), rate constant (K_1 and K_2), and

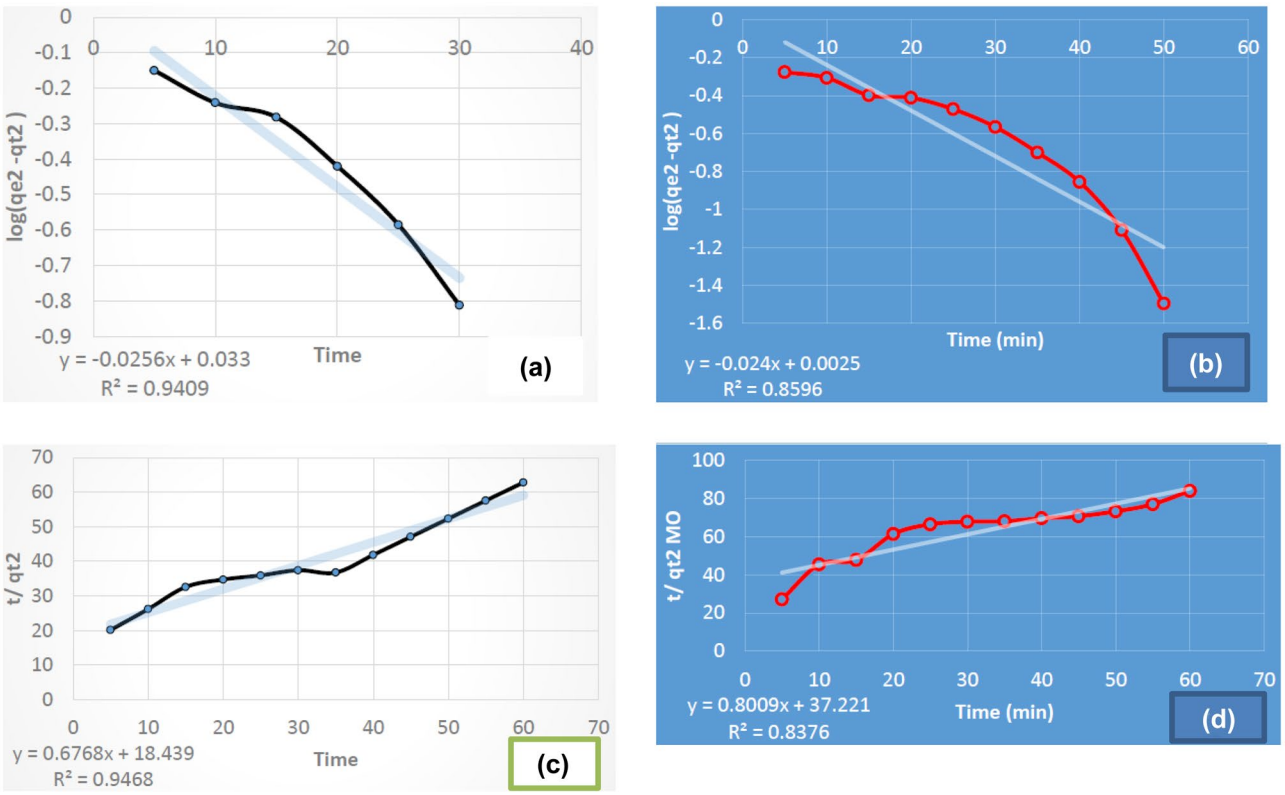

Fig. 14 The pseudo-first-order kinetics nanocomposites GO/HEMA/Fe_3O_4 for adsorption: **a** MB and **b** MO; the pseudo-second-order kinetics nanocomposites GO/HEMA/Fe_3O_4 for adsorption: **c** MB and **d** MO

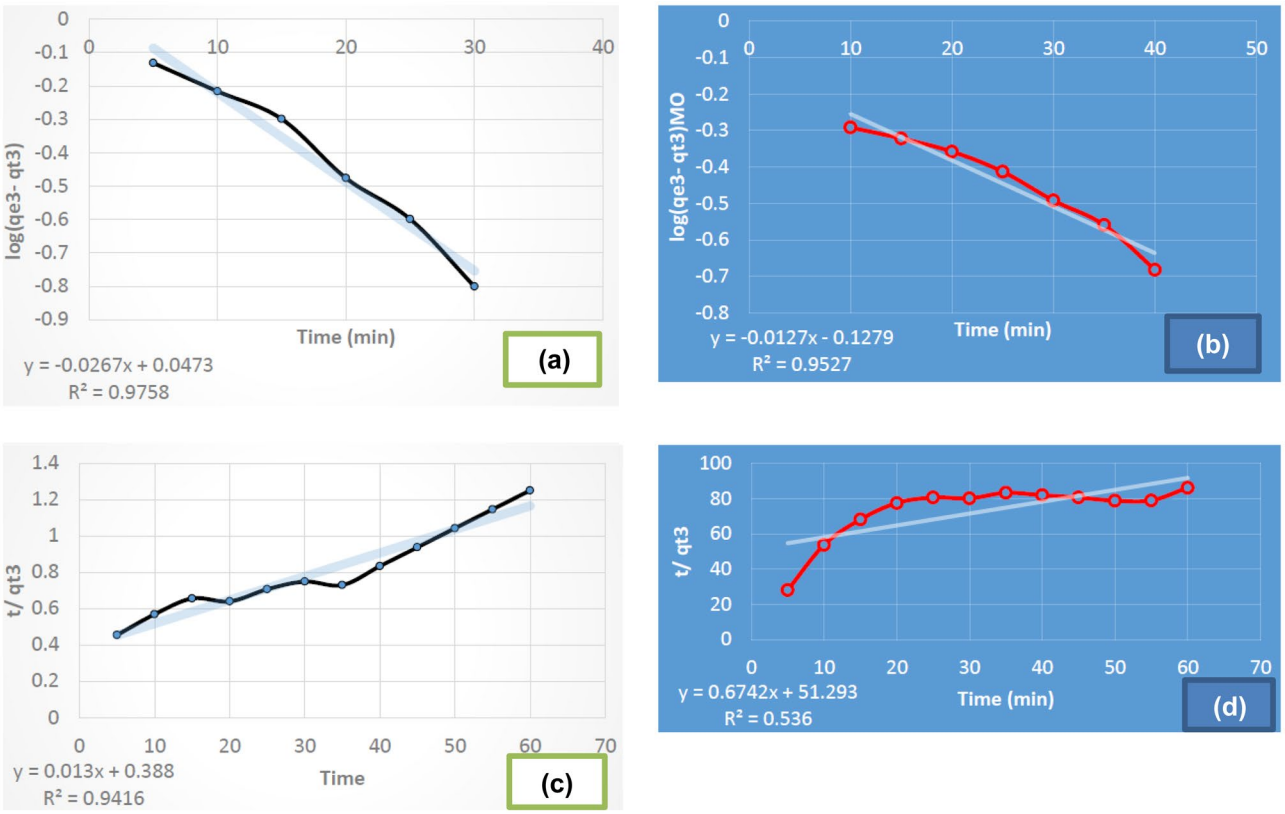

Fig. 15 The pseudo-first-order kinetics nanocomposites GO/HEMA/TiO2 for adsorption: **a** MB and **b** MO; the pseudo-second-order kinetics nanocomposites GO/HEMA/TiO_2 for adsorption: **c** MB and **d** MO

regression coefficients (R^2) are given in Table 2. According to the data in Table 2, the adsorption of dye MB and MO on all three nanocomposite adsorbents is quite appropriate for the first-order-model and more for MB dye. Therefore, we conclude that the removal of pollutants follows the first-order model [53]. The linear shape of the mentioned models is in the form of the following equations [54, 50, 55–60].

$$\log(qe - qt) = \log qe - (K1/2.303).t \tag{6}$$

$$\frac{t}{q_t} = 1/K_2 q_e{}^2 + t/qe \tag{7}$$

where q_e (mg/g) and q_t (mg/g) are the dye capacity absorbed at equilibrium as well as k_1 (min^{-1}), k_2 (g/mg.min), respectively, constant rate of adsorption, pseudo-first-order, and pseudo-second-order.

Table 2 The kinetics constants of dyes adsorption

Adsorbent	Pseudo-first order			Pseudo-second-order		
	$\log(q_e - q_t) = \log q_e - (k_1/2.303)\cdot t$			$t/q_t = 1/k_2.q_e{}^2 + t/q_e$		
	$(q_e)_{Cal}$	k_1	R^2	$(q_e)_{Cal}$	k_2	R^2
MB						
GO/HEMA	0.666	0.0304	0.9846	0.953	0.0301	0.9669
GO/HEMA/Fe_3O_4	1.079	0.0590	0.9409	1.48	0.0250	0.9468
GO/HEMA/TiO_2	1.115	0.0620	0.9758	76.92	0.0004	0.9416
MO						
GO/HEMA	0.461	0.0325	0.9725	0.999	0.0140	0.8450
GO/HEMA/Fe_3O_4	1.006	0.0550	0.8596	1.2496	0.0172	0.8376
GO/HEMA/TiO_2	0.7448	0.2925	0.9527	1.4832	0.0089	0.5360

4 Conclusion

In this study, GO/HEMA, GO/HEMA/Fe_3O_4, and GO/HEMA/TiO_2 nanocomposite materials with GO base were used as adsorbents to remove pollutants (dye MB, MO) from aqueous solutions. GO has a very high adsorption potential due to its very high surface area, free electrons, and OH and COOH functional groups. The polymer from 2-hydroxyethyl methacrylate monomer can be a substrate for GO nanocomposites and prevent them from agglomerating, and it is also a component of green materials. Fe_3O_4 and TiO_2 nanoparticles have high adsorption power and low toxicity. Parameters affecting the removal of pollutants including dye concentration, contact time, and temperature were investigated. According to the obtained results, GO/HEMA, GO/HEMA/Fe_3O_4, and GO/HEMA/TiO_2 nanocomposites are effective adsorbents for MB dye removal compared to GO/HEMA and had good performance at pH = 7. Contaminant removal for all three composites corresponds to the Freundlich isotherm ($R^2 = 0.99$) and first-order kinetics ($R^2 = 0.98$). The dye adsorption mechanism on nanocomposites was obtained by electrostatic interactions, π-π interaction, and hydrogen bonding. For the adsorption kinetics, the high value of R^2 indicates that the adsorption process is chemical and is controlled by the chemical process using hydrogen bonding and π-π accumulation.

Declarations

Conflict of interest The authors declare no competing interests.

References

1. He C, Shi ZQ, Ma L, Cheng C, Nie CX, Zhou M, Zhao CS (2015) Graphene oxide based heparin-mimicking and hemocompatible polymeric hydrogels for versatile biomedical applications. J Mater Chem B 3:592–602. https://doi.org/10.1039/c4tb01806k
2. Benkhaya S, M'rabet S, El Harfi A (2020) A review on classifications, recent synthesis and applications of textile dyes. Inorg Chem Commun 115:107891. https://doi.org/10.1016/j.inoche.2020.107891
3. Panda J, Sahoo JK, Panda PK, Sahu SN, Samal M, Pattanayak SK, Sahu R (2019) Adsorptive behavior of zeolitic imidazolate framework-8 towards anionic dye in aqueous media: combined experimental and molecular docking study. J Mol Liq 278:536–545. https://doi.org/10.1016/j.molliq.2019.01.033
4. Hasanzadeh M, Simchi A, Far HS (2019) Kinetics and adsorptive study of organic dye removal using water-stable nanoscale metal organic frameworks. Mater Chem Phys 233:267–275. https://doi.org/10.1016/j.matchemphys.2019.05.050
5. Saliba D, Ammar M, Rammal M, Al-Ghoul M, Hmadeh M (2018) Crystal growth of ZIF-8, ZIF-67, and their mixed-metal derivatives. J Am Chem Soc 140:1812–1823. https://doi.org/10.1021/jacs.7b11589
6. Benkhaya S, M'rabet S, El Harfi A (2020) Classifications, properties, recent synthesis and applications of azo dyes. Heliyon 6. https://doi.org/10.1016/j.heliyon.2020.e03271
7. Aksu Z, Çağatay ŞŞ (2006) Investigation of biosorption of Gemazol Turquise Blue-G reactive dye by dried Rhizopus arrhizus in batch and continuous systems. Sep Purif Technol 48:24–35. https://doi.org/10.1016/j.seppur.2005.07.017
8. Al-Degs YS, El-Barghouthi MI, El-Sheikh AH, Walker GM (2008) Effect of solution pH, ionic strength, and temperature on adsorption behavior of reactive dyes on activated carbon. Dye Pigment 77:16–23. https://doi.org/10.1016/j.dyepig.2007.03.001
9. Wang C, Liu X, Keser Demir N, Chen JP, Li K (2016) Applications of water stable metal-organic frameworks. Chem Soc Rev 45:5107–5134. https://doi.org/10.1039/c6cs00362a
10. Zhixing Yu, Bai Yu, Wang JH, Li Y (2021) Effects of functional additives on structure and properties of polycarbonate-based composites filled with hybrid chopped carbon fiber/graphene nanoplatelet fillers. ES Energy & Environment 12:66–76
11. Jain B, Singh AK, Hashmi A et al (2020) Surfactant-assisted cerium oxide and its catalytic activity towards Fenton process for non-degradable dye. Adv Compos Hybrid Mater 3:430–441
12. Wu JS, Liu CH, Chu KH, Suen SY (2008) Removal of cationic dye methyl violet 2B from water by cation exchange membranes. J Memb Sci 309:239–245. https://doi.org/10.1016/j.memsci.2007.10.035
13. Lau YY, Wong YS, Teng TT, Morad N, Rafatullah M, Ong SA (2015) Degradation of cationic and anionic dyes in coagulation-flocculation process using bi-functionalized silica hybrid with aluminum-ferric as auxiliary agent. RSC Adv 5:34206–34215. https://doi.org/10.1039/c5ra01346a
14. Kim IC, Lee KH (2006) Dyeing process wastewater treatment using fouling resistant nanofiltration and reverse osmosis membranes. Desalination 192:246–251
15. Lin C, Liu B, Pu L et al (2021) Photocatalytic oxidation removal of fluoride ion in wastewater by g-C3N4/TiO2 under simulated visible light. Adv Compos Hybrid Mater 4:339–349
16. Cheng W, Wang Y, Ge S et al (2021) One-step microwave hydrothermal preparation of Cd/Zr-bimetallic metal–organic frameworks for enhanced photochemical properties. Adv Compos Hybrid Mater 4:150–161
17. Tavassoli N, Ansari R, Mosayebzadeh Z (2017) Synthesis and application of iron oxide/silica gel nanocomposite for removal of sulfur dyes from aqueous solutions. Arch Hyg Sci 6:214–220. https://doi.org/10.29252/archhygsci.6.2.214
18. Cao W, Han M, Qin L et al (2019) Synthesis of zeolitic imidazolate framework-67 nanocube wrapped by graphene oxide and its application for supercapacitors. J Solid State Electrochem 23:325–334. https://doi.org/10.1007/s10008-018-4138-1
19. Yuan B, Li L, Murugadoss V, Vupputuri S, Wang J, Alikhani N, Guo Z (2020) Nanocellulose-based composite materials for wastewater treatment and waste-oil remediation. ES Food & Agroforestry 1:41–52
20. Liu H, Mao Y (2021) Graphene oxide-based nanomaterials for uranium adsorptive uptake. ES Materials and Manufacturing 13:3–22
21. Prashant MK, Avinash R, Kachere N, Mandlik T, Rondiya SR, Jadkar SR, Shivaji V, Bhosale, (2021) Graphene oxide assisted synthesis of magnesium oxide nanorods. ES Materials and Manufacturing 12:63–71
22. Nidamanuri N, Li Y, Li Q, Dong M (2020) Graphene and graphene oxide-based membranes for gas separation. Engineered Science 9:3–16
23. Cai J, Tian J, Hongbo Gu, Guo Z (2019) Amino carbon nanotube modified reduced graphene oxide aerogel for oil/water separation. ES Materials & Manufacturing 6:68–74
24. Singh N, Jana S, Singh GP et al (2020) Graphene-supported TiO2: study of promotion of charge carrier in photocatalytic water splitting and methylene blue dye degradation. Adv Compos Hybrid Mater 3:127–140

25. Cheng C, Liu Z, Li X, Su B, Zhou T, Zhao C (2014) Graphene oxide interpenetrated polymeric composite hydrogels as highly effective adsorbents for water treatment. RSC Adv 4:42346–42357. https://doi.org/10.1039/c4ra07114j
26. Adsorptive removal of toxic dye using Fe3O4−TSC nanocomposite.pdf, (n.d.)
27. Vasile E, Pandele AM, Andronescu C, Selaru A, Dinescu S, Costache M, Hanganu A, Raicopol MD, Teodorescu M (2019) Hema-functionalized graphene oxide: a versatile nanofiller for poly(propylene fumarate)-based hybrid materials. Sci Rep 9:1–7. https://doi.org/10.1038/s41598-019-55081-2
28. Kim SP, Choi HC (2014) Photocatalytic degradation of methylene blue in presence of graphene oxide/TiO2 nanocomposites. Bull Korean Chem Soc 35:2660–2664. https://doi.org/10.5012/bkcs.2014.35.9.2660
29. Mohammad AKT, Abdulhameed AS, Jawad AH (2019) Box-Behnken design to optimize the synthesis of new crosslinked chitosan-glyoxal/TiO 2 nanocomposite: methyl orange adsorption and mechanism studies. Int J Biol Macromol 129:98–109. https://doi.org/10.1016/j.ijbiomac.2019.02.025
30. Bhowmik M, Deb K, Debnath A, Saha B (2018) Mixed phase Fe2O3/Mn3O4 magnetic nanocomposite for enhanced adsorption of methyl orange dye: neural network modeling and response surface methodology optimization. Appl Organomet Chem 32:1–17. https://doi.org/10.1002/aoc.4186
31. Su Z, Zhang M, Lu Z et al (2018) Functionalization of cellulose fiber by in situ growth of zeolitic imidazolate framework-8 (ZIF-8) nanocrystals for preparing a cellulose-based air filter with gas adsorption ability. Cellulose 25:1997–2008. https://doi.org/10.1007/s10570-018-1696-4
32. Shi H, Li W, Zhong L, Xu C (2014) Methylene blue adsorption from aqueous solution by magnetic cellulose/graphene oxide composite: equilibrium, kinetics, and thermodynamics. Ind Eng Chem Res 53:1108–1118. https://doi.org/10.1021/ie4027154
33. Safaiee M, Zolfigol MA, Derakhshan-Panah F, Khakyzadeh V, Mohammadi L (2016) Synthesis of nano magnetite Fe3O4 based vanadic acid: a highly efficient and recyclable novel nanocatalyst for the synthesis of 4,4′-(arylmethylene)-bis(3-methyl-1-phenyl-1H-pyrazol-5-ols). Croat Chem Acta 89:317–322. https://doi.org/10.5562/cca2854
34. Cheng C, Liu Z, Li X, Su B, Zhou T, Zhao C (2014) Graphene oxide interpenetrated polymeric composite hydrogels as highly effective adsorbents for water treatment. RSC Adv 4:42346–42357. https://doi.org/10.1039/c4ra07114j
35. He A, Lei B, Cheng C, Li S, Ma L, Sun S, Zhao C (2013) Toward safe, efficient and multifunctional 3D blood-contact adsorbents engineered by biopolymers/graphene oxide gels. RSC Adv 3:22120–22129. https://doi.org/10.1039/c3ra44775h
36. Zhao S, Wang H (2020) An integrated H-type method to measure thermoelectric properties of two-dimensional Materials 9:59–66
37. Ryu H, Roshan R, Kim MI et al (2017) Cycloaddition of carbon dioxide with propylene oxide using zeolitic imidazolate framework ZIF-23 as a catalyst. Korean J Chem Eng 34:928–934. https://doi.org/10.1007/s11814-016-0339-4
38. Yang N, Zhu S, Zhang D, Xu S (2008) Synthesis and properties of magnetic Fe3O4-activated carbon nanocomposite particles for dye removal. Mater Lett 62:645–647. https://doi.org/10.1016/j.matlet.2007.06.049
39. Shi H, Li W, Zhong L, Xu C (2014) Methylene blue adsorption from aqueous solution by magnetic cellulose/graphene oxide composite: Equilibrium, kinetics, and thermodynamics. Ind Eng Chem Res 53 (2014) 1108–1118. https://doi.org/10.1021/ie4027154
40. Yuan Y, Xu X, Xia J et al (2019) A hybrid material composed of reduced graphene oxide and porous carbon prepared by carbonization of a zeolitic imidazolate framework (type ZIF-8) for voltammetric determination of chloramphenicol. Microchim Acta 186:191. https://doi.org/10.1007/s00604-019-3298-8
41. Babu MJ, Botsa SM, Rani SJ et al (2020) Enhanced photocatalytic degradation of cationic dyes under visible light irradiation by CuWO4-RGO nanocomposite. Adv Compos Hybrid Mater 3:205–212
42. Zhao D, Gao X, Wu C, Xie R, Feng S, Chen C (2016) Facile preparation of amino functionalized graphene oxide decorated with Fe 3 O 4 nanoparticles for the adsorption of Cr(VI). Appl Surf Sci 384:1–9. https://doi.org/10.1016/j.apsusc.2016.05.022
43. Nasrollahzadeh M, Atarod M, Jaleh B, Gandomirouzbahani M (2016) In situ green synthesis of Ag nanoparticles on graphene oxide/TiO2 nanocomposite and their catalytic activity for the reduction of 4-nitrophenol, congo red and methylene blue. Ceram Int 42:8587–8596. https://doi.org/10.1016/j.ceramint.2016.02.088
44. Xu H, Ding M, Chen W, Li Y, Wang K (2018) Nitrogen–doped GO/TiO2 nanocomposite ultrafiltration membranes for improved photocatalytic performance. Sep Purif Technol 195:70–82. https://doi.org/10.1016/j.seppur.2017.12.003
45. Gul S, Sohni S, Waqar M, Ahmad F, Norulaini NAN, MOAK (2016) Functionalization of magnetic chitosan with graphene oxide for removal of cationic and anionic dyes from aqueous solution. Carbohydr Polym 152:520–531. https://doi.org/10.1016/j.carbpol.2016.06.045
46. Paredes A, Acuña SM, Gutiérrez L, Toledo PG (2019) Zeta potential of pyrite particles in concentrated solutions of monovalent seawater electrolytes and amyl xanthate. Minerals 9. https://doi.org/10.3390/min9100584
47. Wang Y, Liang S, Chen B, Guo F, Yu S, Tang Y (2013) Synergistic removal of Pb(II), Cd(II) and humic acid by Fe3O4@Mesoporous silica-graphene oxide composites. PLoS ONE 8:1–9. https://doi.org/10.1371/journal.pone.0065634
48. Au PI, Leong YK (2013) Rheological and zeta potential behaviour of kaolin and bentonite composite slurries. Colloids Surfaces A Physicochem Eng Asp 436:530–541. https://doi.org/10.1016/j.colsurfa.2013.06.039
49. Chen K, He J, Li Y, Cai X, Zhang K, Liu T, Hu Y, Lin D, Kong L, Liu J (2017). Removal of cadmium and lead ions from water by sulfonated magnetic nanoparticle adsorbents. https://doi.org/10.1016/j.jcis.2017.01.082
50. Shojaei S, Khammarnia S, Shojaei S, Sasani M (2017) Removal of Reactive Red 198 by Nanoparticle zero valent iron in the presence of hydrogen peroxide. J Water Environ Nanotechnol 2:129–135. https://doi.org/10.22090/jwent.2017.02.008
51. Arora C, Soni S, Sahu S, Mittal J, Kumar P, Bajpai PK (2019) Iron based metal organic framework for efficient removal of methylene blue dye from industrial waste. J Mol Liq 284:343–352. https://doi.org/10.1016/j.molliq.2019.04.012
52. Pirsaheb M, Hossaini H, Nasseri S et al (2020) Optimization of photocatalytic degradation of methyl orange using immobilized scoria-Ni/TiO2 nanoparticles. J Nanostruct Chem 10:143–159
53. Ali Baig A, Rathinam V, Ramya V (2021) Facile fabrication of Zn-doped SnO2 nanoparticles for enhanced photocatalytic dye degradation performance under visible light exposure. Adv Compos Hybrid Mater 4:114–126
54. Rajabi M, Mahanpoor K, Moradi O (2019) Preparation of PMMA/GO and PMMA/GO-Fe 3 O 4 nanocomposites for malachite green dye adsorption: kinetic and thermodynamic studies. Compos Part B Eng 167:544–555. https://doi.org/10.1016/j.compositesb.2019.03.030
55. Fathi MR, Asfaram A, Farhangi A (2015) Removal of Direct Red 23 from aqueous solution using corn stalks: isotherms, kinetics and thermodynamic studies. Spectrochim Acta - Part A Mol Biomol Spectrosc 135:364–372. https://doi.org/10.1016/j.saa.2014.07.008

56. Kaur D, Bagga V, Behera N et al (2019) SnSe/SnO2 nanocomposites: novel material for photocatalytic degradation of industrial waste dyes. Adv Compos Hybrid Mater 2:763–776
57. Isa EDM, Shameli K, Jusoh NWC et al (2021) Rapid photodecolorization of methyl orange and rhodamine B using zinc oxide nanoparticles mediated by pullulan at different calcination conditions. J Nanostruct Chem 11:187–202
58. örgün N, Özer Ç, Polat K (2019) A new catalyst material from electrospun PVDF-HFP nanofibers by using magnetron-sputter coating for the treatment of dye-polluted waters. Adv Compos Hybrid Mater 2:423–430
59. Huang KY, Wang CT, Chou WL, Shu CM (2013) Removal of polyvinyl alcohol using photoelectrochemical oxidation processes based on hydrogen peroxide electrogeneration. Int J Photoenergy 2013. https://doi.org/10.1155/2013/841762
60. Mahvi AH, Dalvand A (2019) Kinetic and equilibrium studies on the adsorption of Direct Red 23 dye from aqueous solution using montmorillonite nanoclay. Water Qual Res J 1–13. https://doi.org/10.2166/wqrj.2019.008